

## SIMULATION ANALYSIS OF MANIPULATING LIGHT PROPAGATION THROUGH TURBID MEDIA

Snow H. Tseng, Graduate Institute of Photonics and Optoelectronics, National Taiwan University, Taiwan  
stseng@ntu.edu.tw

Liang-Yu Huang, Graduate Institute of Photonics and Optoelectronics, National Taiwan University, Taiwan  
Tzu-Hao Kuo, Graduate Institute of Photonics and Optoelectronics, National Taiwan University, Taiwan

We model light propagation through turbid media by employing the pseudospectral time-domain (PSTD) simulation technique. With specific amplitude and phase, light can be manipulated to propagate through turbid media via multiple scattering. By exploiting the flexibility of the PSTD simulation, we analyze factors that contribute to enhancing light penetration. Specific research findings suggest that it is possible to propagate light with specific amplitude/phase. The reported simulation analysis enables quantitative analyses of directing light through turbid media.

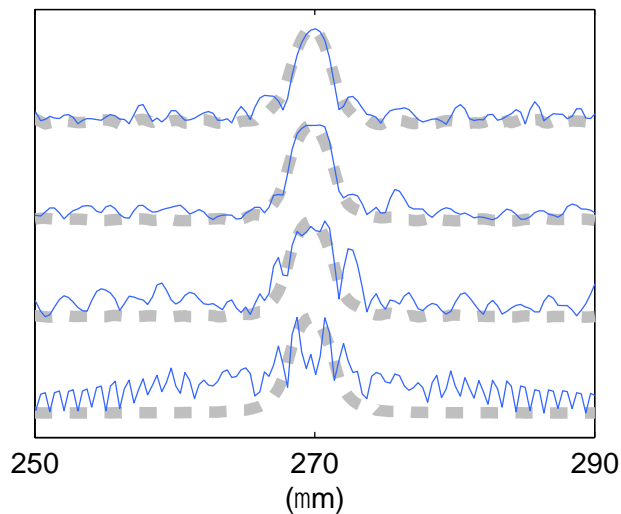


Figure 1. Comparing the transmitted light profile through turbid medium consisting of  $N$  scatterers. (From bottom to top): the turbid medium consists of  $N = 0, 20, 100,$  and  $250$  scatterers, respectively. The transmitted light profile (blue line) is compared to the original source profile (gray dashed line).

## SPECKLEPLETHYSMOGRAPHIC (SPG) ESTIMATION OF HEART RATE VARIABILITY

Cody E. Dunn, Beckman Laser Institute and Medical Clinic, University of California, Irvine (UCI)  
cedunn@uci.edu

Derek C. Monroe, Department of Neurology, UCI

Christian Crouzet, Beckman Laser Institute and Medical Clinic, UCI

James W. Hicks, Department of Ecology and Evolutionary Biology, UCI

Bernard Choi, Beckman Laser Institute and Medical Clinic, UCI

Key Words: Speckleplethysmography, Photoplethysmography, Heart Rate Variability.

Heart rate variability (HRV), a class of metrics derived from variability in R-R intervals typically measured using electrocardiography (ECG), has implications for cardiovascular and neurological health<sup>1</sup>. Recently, HRV was used to track the recovery of athletes after exercise training due to its ability to noninvasively monitor the autonomic nervous system (ANS)<sup>2</sup>. Exercise training generally has a positive impact on the ANS by reducing resting heart rate and increasing cardiac vagal tone at rest<sup>3</sup>. However, overexertion from excessive workout sessions can counteract the benefits of regular exercise and reduce HRV<sup>4</sup>.

Unfortunately, routine, remote ECG HRV monitoring is limited due to portability, cost, and loss of accuracy. Various groups have attempted to address the limitations of ECG monitored HRV by estimating HRV with simpler photoplethysmography (PPG) technology<sup>5</sup>. Transmittance PPG, the signal used in pulse oximetry, measures changes in intensity due to light absorption caused by the dilation and constriction of arteries and arterioles in the finger due to pulsatile blood flow. Alas, HRV approximated from PPG finger measurements loses accuracy due to significant peak time delays related to various factors such as arterial stiffness, vascular tone, and height<sup>6</sup>.

Speckleplethysmography (SPG), a coherent optical signal that measures changes in blood flow using laser speckle imaging, is an inexpensive, early-stage technology, not yet tested for HRV, that has a higher signal-to-noise ratio<sup>7</sup> and robustness in the presence of motion artifact and cold temperatures, when compared to PPG<sup>8</sup>. In addition, the SPG waveform peaks before the PPG waveform, which should improve accuracy and reduce the impact of vascular compliance on HRV estimation.

Given the aforementioned benefits of SPG, we studied the relationship of SPG and PPG to ECG for estimation of HRV during an orthostatic challenge performed by 17 subjects. We found that SPG estimations of HRV are highly correlated to ECG HRV for both time and frequency domain parameters (Fig. 1) and provide improvements over PPG estimations of HRV. For 11 out of 12 HRV parameters, the correlation coefficients for SPG and ECG are greater than the correlation coefficients for PPG and ECG.

The results suggest SPG measurements are a viable alternative for HRV estimation when ECG measurements are impractical.

The two most relevant topics for the abstract are Imaging through Turbid Media and Optics and Biomechanics. The information is relevant to the conference because it provides a new translational application of a photonic technology, with *in vivo* results for the SPG technique.

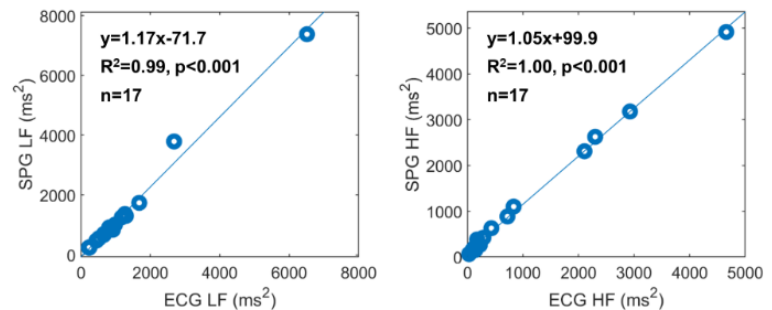


Figure 1 – SPG and ECG data collected from 17 subjects while standing. Waveforms were bandpass filtered to extract low-frequency (LF) and high-frequency (HF) contributions to the waveforms. The data show a strong correlation.

1. Thayer, J. F., et al. *Neurosci. Biobehav. Rev.* 36, 747–756 (2012).
2. Dong, J. G. *Exp. Therapeut. Med.* 11, 1531-1536 (2016).
3. Seals, D. R. & Chase, P. B. *J. Appl. Physiol.* 66, 1886–1895 (1989).
4. Flatt, A. et al. *J. Strength Cond. Res.* 32, 3127–3134 (2018).
5. Schäfer, A. & Vagedes, J. *Int. J. Cardiol.* 166, 15–29 (2013).
6. Charlott, K., et al. *Physiol. Meas.* 30, 1357–1369 (2009).
7. Dunn, C. E., et al. *Biomed. Opt. Express* 9, 4306-4316 (2018).
8. Ghijssen, M., et al. *Biomed. Opt. Express* 9, 3937–3952 (2018).

## **MODEL EYE IMAGING BY CLOSED-LOOP ACCUMULATION OF SINGLE SCATTERING (CLASS) MICROSCOPY**

Yookyung Jung, Center for Molecular Spectroscopy and Dynamics, Institute for Basic Science (IBS), Korea;  
Center for Systems Biology and Wellman Center for Photomedicine, Massachusetts General Hospital and  
Harvard Medical School, USA  
omeletjung@korea.ac.kr

Pilsung Kang, Center for Molecular Spectroscopy and Dynamics, Institute for Basic Science (IBS); Department  
of Physics, Korea University, Korea

Yongwoo Kwon, Center for Molecular Spectroscopy and Dynamics, Institute for Basic Science (IBS);  
Department of Physics, Korea University, Korea

Jin Hee Hong, Center for Molecular Spectroscopy and Dynamics, Institute for Basic Science (IBS); Department  
of Physics, Korea University, Korea

Wonshik Choi, Center for Molecular Spectroscopy and Dynamics, Institute for Basic Science (IBS); Department  
of Physics, Korea University, Korea

'Closed-loop accumulation of single scattering (CLASS)' microscopy provides novel solutions to the problems of light scattering and aberration in optical imaging, providing increased imaging depth while maintaining diffraction limited resolution. This method has a great potential to increase imaging depth and resolution of current eye imaging. In this presentation, the strength and weakness of the CLASS microscopy over the current adaptive optical microscopy will be discussed. Important factors to apply CLASS microscopy to eye imaging and the possibility to imaging retina in turbid condition will be discussed by using model eye.

## INTERFEROMETRIC SPECKLE VISIBILITY SPECTROSCOPY FOR IMPROVED MEASUREMENT OF BLOOD FLOW DYNAMICS

Joshua Brake, Dept. of Electrical Engineering, California Institute of Technology, USA  
jbrake@caltech.edu

Jian Xu, Dept. of Electrical Engineering, California Institute of Technology, USA  
Ali Kazemi Jahromi, Dept. of Electrical Engineering, California Institute of Technology, USA  
Changhui Yang, Dept. of Electrical Engineering, California Institute of Technology, USA

Key Words: scattering, diffuse correlation spectroscopy, interferometry, speckle, blood flow

The dynamics of blood flow within tissue is a key indicator of metabolic function, providing functional information about physiological activity [1]. Speckle visibility spectroscopy (SVS) [2,3] is an emerging technique which allows for blood flow dynamics to be measured non-invasively by analyzing the statistical properties of a captured optical speckle field which has interacted with blood in a volume of interest. Blurring of the speckle field caused by the dynamic scattering of the blood cells contains information about the blood flow dynamics. However, at weak signal light intensities, the impact of camera noise prevents accurate measurements of the sample dynamics using SVS. This means that longer camera exposures are required in order to accumulate enough signal photons to accurately determine the dynamics of the sample, which leads to reduced measurement refresh rates.

In this poster we will present an optical measurement method which enables high-speed measurement of the optical field dynamics with shot-noise limited sensitivity. This method, termed interferometric speckle visibility spectroscopy (iSVS), enables sensitive, non-invasive monitoring of hemodynamic activity, even when dealing with very weak signal light intensities. Furthermore, the interferometric nature of the measurement allows for calculations to be performed with the electric field autocorrelation function  $g_1(t)$  directly, avoiding the errors typically encountered when relating the intensity autocorrelation function  $g_2(t)$  to the blood flow signal of interest and enabling accurate measurements in samples where the scattering dynamics are non-ergodic. In this poster we will develop the theoretical advantages of iSVS compared to other methods for measuring blood flow in dynamic samples and also present some proof-of-concept *in-vivo* blood flow data collected from rodent models.

### References:

- [1] Durduran, Turgut, and Arjun G. Yodh. "Diffuse correlation spectroscopy for non-invasive, micro-vascular cerebral blood flow measurement." *Neuroimage* 85 (2014): 51-63.
- [2] Dixon, P. K., and Douglas J. Durian. "Speckle visibility spectroscopy and variable granular fluidization." *Physical review letters* 90.18 (2003): 184302.
- [3] Bandyopadhyay, Ranjini, et al. "Speckle-visibility spectroscopy: A tool to study time-varying dynamics." *Review of scientific instruments* 76.9 (2005): 093110.

## GENERATIVE ADVERSARIAL NETWORK PREDICTION OF OPTICAL PROPERTIES FROM SINGLE IMAGES WITH STRUCTURED- OR HOMOGENOUS-ILLUMINATION

Nicholas J. Durr, Department of Biomedical Engineering, Johns Hopkins University  
ndurr@jhu.edu

Tianyi Chen, Department of Biomedical Engineering, Johns Hopkins University  
Jordan Sweer, Department of Biomedical Engineering, Johns Hopkins University  
Faisal Mahmood, Department of Biomedical Engineering, Johns Hopkins University

Key Words: optical properties, spatial frequency domain imaging, deep learning, adversarial networks.

We present a deep learning approach for mapping absorption and scattering coefficients from widefield images, called Generative Adversarial Network Prediction of Optical Properties (GANPOP). This approach is purely data-driven—no assumptions or models of light-tissue interaction are used. We obtain a series of ground truth reduced scattering and absorption coefficient maps from tissue phantoms, ex-vivo pig gastrointestinal tissues, and ex-vivo human esophagus samples using Spatial Frequency Domain Imaging (SFDI). SFDI was performed at 660 nm with a three-phase ( $0$ ,  $2/3 \pi$ , and  $4/3 \pi$ ) and two spatial frequency ( $0$  and  $0.2 \text{ mm}^{-1}$ ) strategy. The training set comprised nine different tissue phantoms and seven ex-vivo human esophagus samples. For testing, nine phantoms, four pig samples, and one human esophagus specimen were used. Patches of paired optical properties and raw acquired images were used to simultaneously train a Generator that estimates realistic optical properties given a conventional image, and a Discriminator that learns to classify real versus predicted image pairs. After training is complete, the Generator is used to estimate optical properties from an input of a single widefield image along with three constant calibration images. Compared to model-based approaches, such as Single Snapshot Optical Properties (SSOP), GANPOP estimates both reduced scattering and absorption coefficients in human esophagus with an approximately 50% smaller root-mean-square error when given a  $0.2 \text{ mm}^{-1}$  spatial frequency input image [Figure 1]. Interestingly, GANPOP also produces a closer estimate of optical properties to the SFDI ground truth from a homogenous illumination image than SSOP estimates from structured light. When tested on pig tissues, which represent an organism completely unrepresented in the training set, GANPOP estimates optical properties with similar error rates to SSOP. These results suggest that, given relevant training, GANPOP can improve accuracy of single snapshot optical properties from structured illumination images. Furthermore, GANPOP may enable optical property mapping from conventional flood-illuminated images, raising the possibility that optical properties can be mapped using images obtained from unmodified commercial endoscopes.

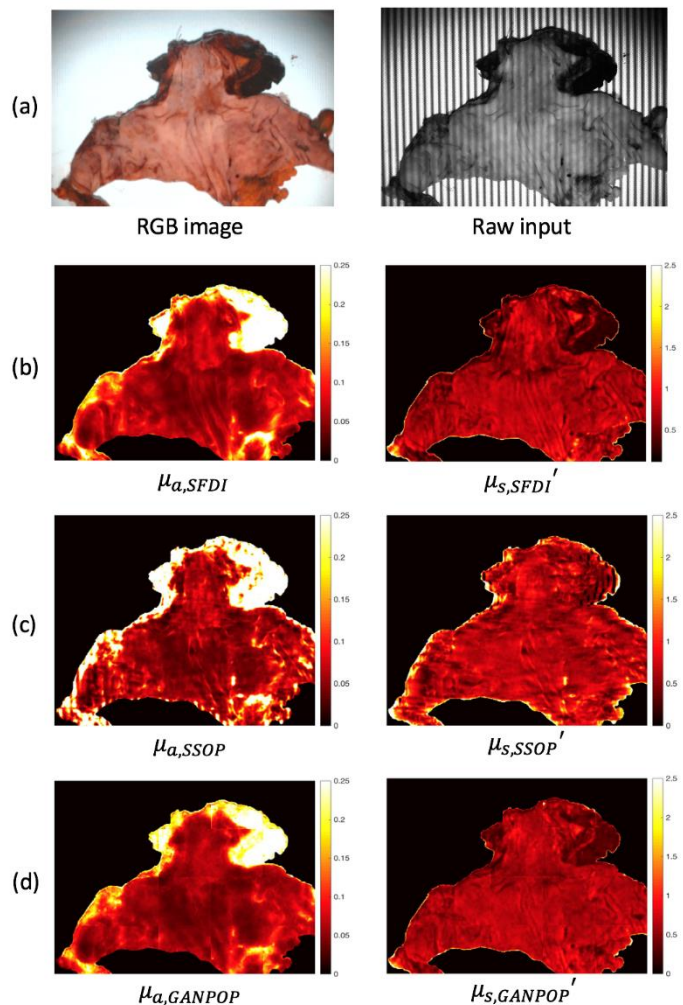


Figure 2: Example results for ex vivo human sample. Row (a): RGB and raw input structured illumination image; (b) ground truth; (c) SSOP results; (d) GANPOP results; All values are measured in  $\text{mm}^{-1}$ .

## DE-SCATTERING WITH EXCITATION PATTERNING IN TEMPORALLY-FOCUSED MICROSCOPY (DEEP-TFM)

Jong Kang Park, Department of Biological Engineering, Massachusetts Institute of Technology, USA  
jongpark@mit.edu

Dushan N. Wadduwage, Center for Advanced Imaging, Faculty of Arts and Sciences, Harvard University, USA  
Peter T. C. So, Department of Biological Engineering, Department of Mechanical Engineering, Laser Biomedical Research Center, Massachusetts Institute of Technology, USA

**Key Words:** Nonlinear microscopy, Fluorescence microscopy, Tissue imaging, Scattering, Computational imaging.

Point-scanning two-photon microscopy is used routinely for *in vivo*, volumetric biological imaging, especially in deep tissues. Despite the excellent penetration depth, a conventional point-scanning two-photon microscopy is slow due to the need for raster scanning and imaging time scales linearly with increasing volume, hampering studies of fast biological dynamics. An attractive alternative to point-scanning geometries is wide-field two-photon microscopy, typically called temporal focusing microscopy (TFM) since optical sectioning is achieved by focusing a beam temporally while maintaining wide-field illumination. However, TFM suffers from scattering in tissue resulting in limited imaging depth.

We introduce a novel computational de-scattering technique called De-scattering by Excitation Patterns in TFM or 'DEEP-TFM'. We use wide-field temporal focusing patterned excitation and the signal is measured with a wide-field detector, such as a camera. Briefly, we built a modified temporal focusing microscope that projects arbitrary excitation patterns onto the focal plane using a digital mirror device (DMD). Emission light from the modulated excitation is then detected by a camera. Due to their NIR wavelengths, the excitation patterns maintain their fidelity despite travelling through scattering medium. However, the emission photons are scattered by tissues and the strength of scattering is strongly depth dependent. This assumption holds for most biological tissue. In practice, TFM images are minimally affected by scattering at or near the surface; as the imaging depth increases, scattering gradually degrades high-frequency information in the images. However, low frequencies in the images are retained for most depths even with wide-field detection. Single pixel detection approaches discard this low frequency information, and hence require a large number of excitation patterns. We then combine the information about the excitation patterns with the acquired images, to computationally reconstruct a de-scattered image. Experimentally, to de-scatter a single FOV, multiple patterned excitations (and images) are needed; the number depends on the loss of high-frequency information due to scattering, and hence on the imaging depth.

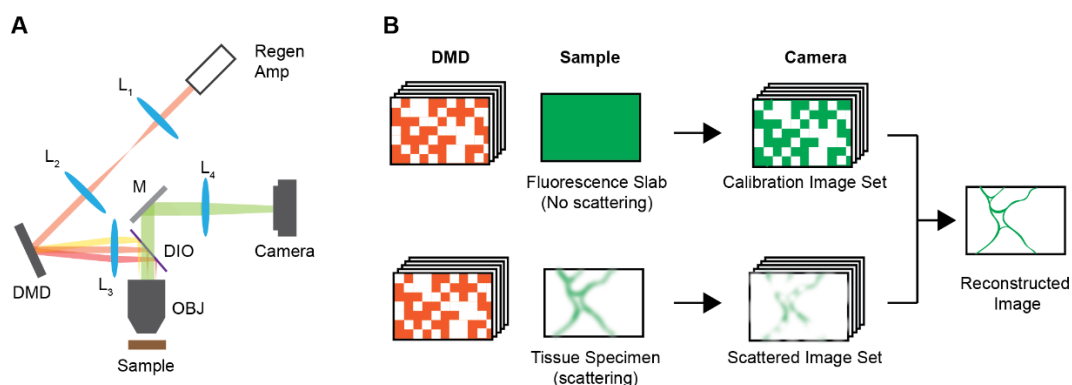


*Figure 3. (A) Optical schematic of the imaging system: L1, L2, L3, L4 – lenses; DMD- Digital Mirror Device; DIO – Dichroic mirror; OBJ – Microscope objective. (B) Proposed computational imaging strategy. First a set of patterns are projected on a calibration specimen (homogeneous thin fluorescent layer) to record the calibration image set at the absence of any scattering. Then the same patterns are projected to record the encoded images through a scattering medium. Then the de-scattered images are reconstructed.*

# UTILIZING ECTOPIC HSP90 EXPRESSION TO DIAGNOSE BREAST CANCER AT THE POINT-OF-CARE USING FLUORESCENCE MICROSCOPY

Roujia Wang, Biomedical Engineering, Duke University  
roujia.wang@duke.edu  
Brian Crouch, Biomedical Engineering, Duke University  
Christopher Lam, Biomedical Engineering, Duke University  
Jenna Muller, Biomedical Engineering, Duke University  
Philip Hughes, Duke University School of Medicine  
Timothy Haystead, Duke University School of Medicine  
Nimmi Ramanujam, Biomedical Engineering, Duke University

**Key Words:** Molecular imaging, fluorescence microscopy, Hsp 90 inhibitors, breast cancer diagnosis

Although pathological examination serves as the gold standard for breast cancer diagnosis, it requires labor-intensive sample preparation and time-consuming evaluation, resulting in long turn-around time and extensive infrastructure. We have developed a simple molecular imaging platform that can quickly assess patient's samples and provide a molecular signal to reflect disease pathology as an alternative to traditional pathology, particularly for applications in low resource settings. We identified Heat shock protein 90 (Hsp90) as a molecular target to diagnose breast cancer as it is overexpressed on the surface of all breast cancer cell subtypes to orchestrate stress response to cancer formation. Based on this feature, we have established a non-invasive and rapid molecular imaging approach to quantify Hsp90 expression on breast tissue biopsies using a FITC tethered Hsp90 inhibitor (HS-27) that binds to surface Hsp90 of breast cancer cells. A wide-field, high resolution, handheld fluorescent microscope referred to as the Pocket Mammoscope has been developed to perform rapid non-contact Hsp90 fluorescent imaging of entire tissue biopsies at point of care.

The Pocket Mammoscope uses a concentric excitation blue LED source ( $470\pm 20$  nm) a band-pass emission filter ( $534\pm 26$ nm) for HS-27 fluorescence emission and a CMOS detector for imaging (Figure 1A). It is capable of 3-52X magnification and can perform both wide-field and high-resolution imaging by changing the working distance using a user-controlled slider mechanism on the body of the scope. In wide-field imaging mode, the Pocket Mammoscope achieves a FOV of 35 mm and an optical resolution of  $24.8\ \mu\text{m}$  while high-resolution mode achieves a FOV of 8.5 mm and an optical resolution of  $8.77\ \mu\text{m}$ . This dual imaging mode of Pocket Mammoscope allow us to image entire region of a core needle biopsy in one snapshot using the wide-field mode and zoom in to the regions of interest using a high-resolution mode (Figure 1B).

In our pilot clinical studies, we also demonstrated the feasibility of using the Pocket Mammoscope for Hsp90 fluorescent imaging on patient breast core needle biopsies. We showed that HER2+ biopsy has significantly higher HS-27 signal compared to benign breast tissues (Figure 1C). To examine the sensitivity and specificity of Hsp90 imaging, we used features from the image in a Gaussian support vector machine (GSVM) classifier. A Receiver Operating Characteristics (ROC) curve shows specificity (100%) and sensitivity (86%) of Hsp90 for distinguishing malignant tumor biopsies ( $n = 27$ ) from benign biopsies ( $n = 10$ ) (Figure 1D). We are further optimizing our Hsp90 staining protocol and prototyping an automated staining platform to ensure uniform and consistent staining and washing of clinical biopsy samples as a way to improve sensitivity. By integrating an automated staining platform with Pocket Mammscope, our diagnostic platform could ultimately serve as an alternative to traditional pathology at a point-of-care setting.

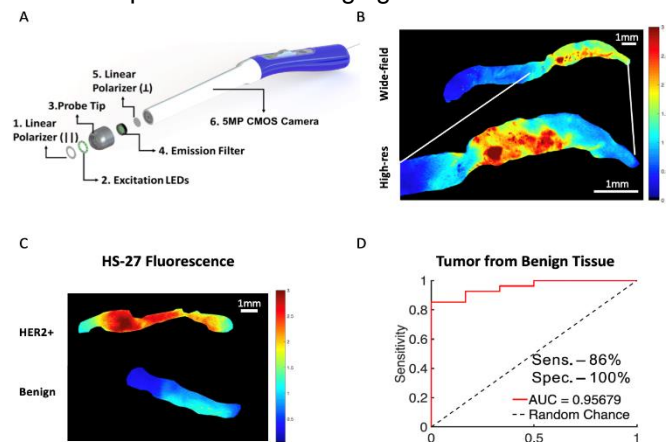


**Figure 4 – (A) Pocket Mammoscope: (1) first linear film polarizer (2) concentric illumination with LEDs ( $470\pm 20$  nm) (3) aluminum holder (4) emission filter ( $535\pm 26$ nm) (5) second linear film polarizer. (B) Representative image of cancerous breast biopsy captured by Pocket Mammoscope in wide-field (left) and high-resolution (right) modes. (C) Representative image of patient breast biopsies captured by Pocket Mammoscope: HER2+ (top) and Mammoplasty (bottom). (D) HS-27 ROC for distinguishing malignant tumor from benign tissue based on the top 1% of pixels**

# MATRIX APPROACH OF FULL-FIELD OCT FOR VOLUMETRIC IMAGING OF AN OPAQUE HUMAN CORNEA

Paul Balondrade, Institut Langevin, ESPCI Paris, PSL University, France  
paul.balondrade@espci.fr

Victor Barolle, Institut Langevin, ESPCI Paris, PSL University, France

Ulysse Najar, Institut Langevin, ESPCI Paris, PSL University, France

Claude Boccara, Institut Langevin, ESPCI Paris, PSL University, France

Mathias Fink, Institut Langevin, ESPCI Paris, PSL University, France

Alexandre Aubry, Institut Langevin, ESPCI Paris, PSL University, France

Kristina Irsch, Institut de la Vision, UPMC-Sorbonne Universities, Quinze-Vingts National Eye Hospital, France

Key Words: Microscopy, OCT, Matrix approach, Imaging through Turbid Media

Optical microscopy offers the possibility to image biological tissue with a diffraction limited resolution ( $\sim\mu\text{m}$ ). However, the heterogeneity of biological tissues can strongly affect light propagation at large depths by distorting the initial wavefront. Large and short range fluctuations of the refractive index can induce aberration and multiple scattering, respectively. Inspired by a recent work [1], we have developed a matrix approach to Full-Field Optical Coherence Tomography (FF-OCT) to push back the fundamental limit of aberrations and multiple scattering. Here, we report on the application of this approach to the imaging of the human cornea and the quantitative measurement of the corneal transparency.

The matrix approach for FF-OCT is based on the measurement of a time-gated reflection matrix  $R$ . Each element of  $R$  corresponds to the impulse response between a point in a source and an image plane respectively, both conjugated to the sample plane. From  $R$ , we are able to recover a confocal image as well as an average focal spot. This reflection matrix can be used to measure the amount of aberration that the incident wavefront has undergone inside the medium.

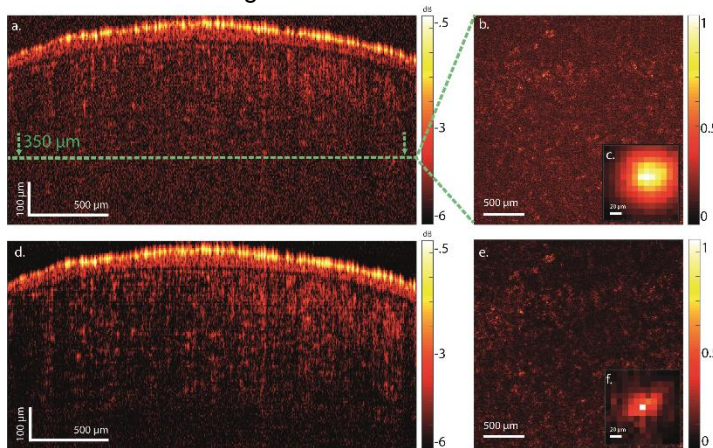


*Figure 5 – Aberration correction for imaging of a human cornea. a. Axial section of the FF-OCT image (in dB) of the cornea without and d. with correction for aberration. b, f. En-face FF-OCT image of the cornea at a depth of 350 mm before and after correction, respectively. c, f. Average focal spot deduced from  $R$  at the depth of 350 mm before and after correction, respectively.*

We measured  $R_z$  as a function of depth in an ex-vivo human cornea. As light propagates inside the cornea, it undergoes strong phase distortion that severely degrades the quality of the FF-OCT image (Fig 1 a. and b.). This distortion can be clearly observed on the spreading of the focal spot (Fig 1 c.). Conventional adaptive optics allows to correct for one part of the image but is not efficient over the whole FOV. Conversely, our matrix approach yields a high-quality image of the cornea over the whole FOV as if the inhomogeneities of the cornea had disappeared (Fig 1 d. and e.). Furthermore, the recovery of a diffraction limited PSF (Fig 1 f.) proves the success of the correction. This approach also allows a quantitative measurement of the scattering mean free path,  $l_s$ , inside the different layers of the cornea. This parameter is relevant to characterize corneal transparency, which can be impacted by several diseases such as keratoconus.

The perspective of this work is to go beyond cornea and apply our approach to retinal and choroidal imaging. In addition, as this matrix approach is not limited to the study of the eye, future work will be applied to in-depth imaging of biological tissues.

## References

1. A. Badon, D. Li, G. Lerosey, A. C. Boccara, M. Fink, A. Aubry "Smart optical coherence tomography for ultra-deep imaging through highly scattering media," *Sci. Adv.* 2, e1600370 (2016).

## IMAGE-GUIDED FLUORESCENCE TOMOGRAPHY IN HEAD & NECK SURGICAL MODELS

Michael J. Daly, TECHNA Institute, University Health Network  
michael.daly@uhn.ca

Harley Chan, TECHNA Institute, University Health Network  
Brian C. Wilson, University Health Network & University of Toronto  
Jonathan C. Irish, University Health Network & University of Toronto  
David A. Jaffray, University Health Network & University of Toronto

Key Words: molecular-guided surgery; fluorescence tomography; cone-beam CT; surgical navigation

Clinical indications for fluorescence-guided surgery continue to expand, and are being spurred by the rapid development of new agents that improve biological targeting.<sup>1</sup> There is a corresponding need to develop imaging systems that quantify fluorescence – not only at the tissue surface, but at depth. We have recently described an image-guided fluorescence tomography system that leverages geometric data from intraoperative cone-beam CT and surgical navigation,<sup>2</sup> and builds on finite-element method software (NIRFAST) for diffuse optical tomography (DOT).<sup>3</sup> DOT systems have most commonly been used for sub-surface inclusions buried within tissue (e.g., breast and neurological tumors). Here, we focus on inclusion models relevant to tumors infiltrating from the mucosal surface (an “iceberg” model), as is most often the case in head and neck cancer, where over 85% of tumors are squamous cell carcinoma.<sup>4</sup> This work presents results from simulations, tissue-simulating anatomical phantoms, and animal studies involving infiltrative tumor models. The objective is to characterize system performance across a range of inclusion diameters, depths, and optical properties. For example, Fig. 1 shows a fluorescence reconstruction of a simulated tonsil tumor in an oral cavity phantom. Future clinical studies are necessary to assess *in vivo* performance and intraoperative workflow.

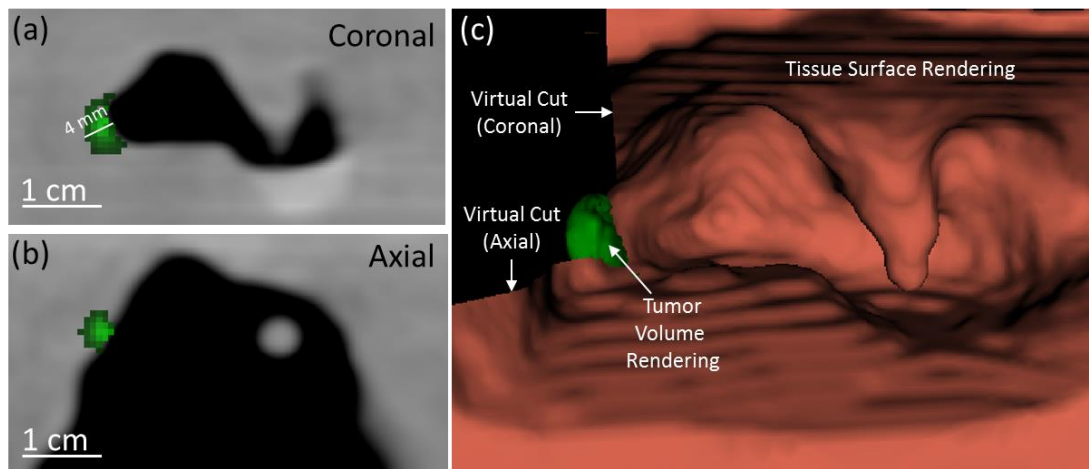


Figure 6 – Fluorescence reconstruction in a trans-oral surgery lab model. Cone-beam CT slices for (a) coronal and (b) axial views with fluorescence overlay showing estimated depth of tumor invasion (~4 mm). (c) Virtual clipping planes reveal fluorescence volume infiltrating below tissue surface.

1. Tipirneni KE, Warram JM, Moore LS, et al. Oncologic Procedures Amenable to Fluorescence-guided Surgery. *Ann Surg.* 2017;266(1):36-47.
2. Daly MJ, Chan H, Muhanna N, et al. Non-contact fluorescence tomography with a cone-beam CT surgical guidance system. Paper presented at: Proc. SPIE2019; San Francisco, CA.
3. Dehghani H, Eames ME, Yalavarthy PK, et al. Near infrared optical tomography using NIRFAST: Algorithm for numerical model and image reconstruction. *Commun Numer Methods Eng.* 2008;25(6):711-732.
4. Mehanna H, West CM, Nutting C, Paleri V. Head and neck cancer--Part 2: Treatment and prognostic factors. *Bmj.* 2010;341:c4690.

# A FAST THREE-DIMENSIONAL DYNAMIC LIGHT SCATTERING COMPUTATIONAL MODEL FOR IMAGING THROUGH HETEROGENOUS TURBID MEDIA

Chakameh Z. Jafari, The University of Texas at Austin, USA  
 cjafari@utexas.edu

David R. Miller, Colin T. Sullender, Samuel A. Mihelic, Andrew K. Dunn, The University of Texas at Austin, USA

Key Words: Laser Speckle Contrast Imaging, Dynamic Light Scattering, Parallelized Monte Carlo, Imaging through Turbid media, Non-invasive blood Flow monitoring

We present a fast numerical Monte Carlo based method (DLS-MC) to rapidly simulate and model dynamic light scattering through three-dimensional heterogeneous tissue volume. Speckle Contrast Imaging (LSCI) uses spatiotemporal fluctuations of random interference patterns of scattered coherent light known as speckle to measure blood flow non-invasively at a micron scale. Laser speckle intensity fluctuations are captured with a camera, and relative blood flow in tissue is analytically inferred by making assumptions about the form of the electric field autocorrelation function<sup>1</sup>. However, in the intermediate regime between the single and multiple scattering such as in tissue, the form of electric field autocorrelation function ( $g_1$ ) is complex and sample-dependent, leading to erroneous measurements if generalized<sup>2</sup>. We use our model to directly compute  $g_1$  without explicit assumptions on its form, furthering our understanding of depth and geometry dependent blood flow variations on the observed Speckle Contrast Image. Additionally, this highly scalable technique is capable of rapidly modeling, in the order of a few seconds, the effect of three-dimensional particle motion perturbations (*i.e.*, blood flow), thus making it feasible to be used as an accurate forward model in volumetric blood flow inverse reconstruction, given that the geometry is known a-priori.

The underlying physics governing the DLS-MC simulations assumes a plane wave electric field incident on the surface of a medium. The resulting back scattered electric field at each detector has a phase shift that is the superposition of the momentum transfer contribution from each detected photon that underwent dynamic scattering<sup>2</sup>. The electric field auto correlation function can then be calculated if the photon scattering positions and angles as well as velocity tensors at scattering locations are known. DLS-MC uses a 3D voxel based Monte Carlo simulator to statistically model the photon trajectories based on the optical properties of the tissue at each voxel. Once photon trajectories and path length dependent absorption weights are calculated, the same model can be perturbed rapidly in a secondary simulation step to calculate  $g_1$  for varying particle flow (*i.e.*, red blood cell) speeds. We computed a speckle contrast image of mouse cerebral blood flow for a 60 x 60 detector grid emulating a camera pixel array, and validated our results against experimental data as shown in Figure 1. We used the Message Passing Interface (MPI) to highly parallelize each simulation step; It took 5 mins of processing time to simulate two billion photon trajectories in the 3D Monte Carlo step on 200 cores at Texas Advanced Computing Center (TACC) and 15 sec of processing time for calculating  $g_1$  for the detector grid.

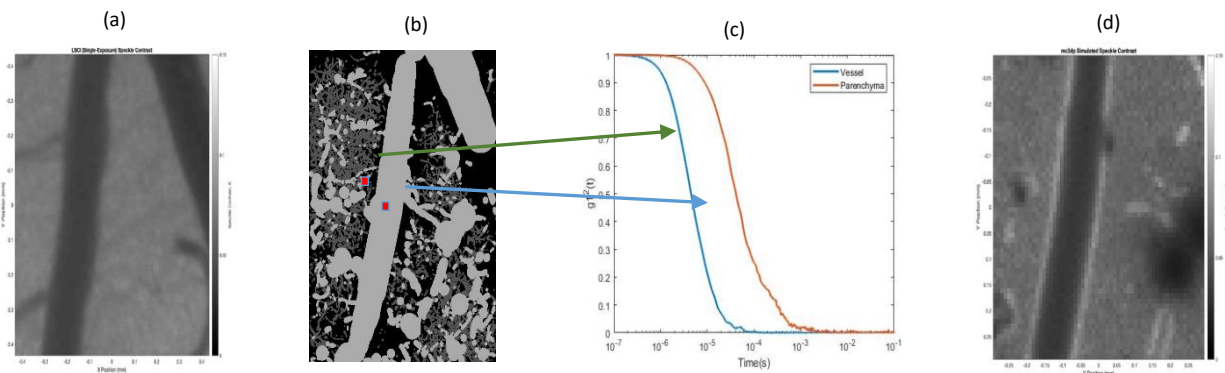


Figure 7. Measured Speckle Contrast Image of a mouse cerebral blood flow (a) Vectorized Maximum Intensity Projection of the same 1mm<sup>3</sup> volume captured through two photon imaging (b) Simulated electric field auto-correlation function for two small detector regions (vessel and parenchyma) (c) Simulated Speckle contrast for a 60x60 detector grid with a 10 μm<sup>2</sup> unit detector size (d)

[1] R. Bandyopadhyay, A. Gittings, S. Suh, P. Dixon, and D. Durian, "Speckle-visibility spectroscopy: A tool to study time-varying dynamics," Review of Scientific Instruments 76, 093,110 (2005)  
 [2] M. A. Davis, S. M. S. Kazmi, and A. K. Dunn, "Imaging depth and multiple scattering in laser speckle contrast imaging," J. Biomed. Opt. 19(8), 086001 (2014)

## CORTEX-WIDE, CELLULAR-RESOLUTION TWO-PHOTON MICROSCOPY

Hunter B. Banks, Washington University in St. Louis  
hbanks@wustl.edu

Jon R. Bumstead, Washington University in St. Louis  
Lindsey M. Brier, Washington University in St. Louis  
Annie Bice, Washington University in St. Louis  
Joseph P. Culver, Washington University in St. Louis

Key Words: Two-photon microscopy, Functional calcium neuroimaging, Photodamage

Functional imaging of the mouse brain in its extreme complexity involves substantial trade-offs. An optical intrinsic spectroscopy system can image the entire cortex but at the expense of spatial and temporal resolution [1]. A two-photon microscope (TPM) can image single neurons with high temporal resolution, but the field of view (FOV) is generally restricted. Advanced techniques like random-access scanning allow for imaging single neurons that are millimeters apart but only by ignoring the neurons and tissue in between [2]. By carefully considering the properties of the optical components as well as the imaging requirements, we present a TPM capable of imaging nearly the entire mouse cortex with 15 Hz frame rates and single neuron resolution.

Designing an effective calcium imaging TPM requires paying careful attention to the optical components, which determine the FOV and resolution, and the properties of the fluorophore, which determine the requisite signal-to-noise ratio (SNR) and frame rate. As in any laser scanning microscope, the galvanometers and relay lenses must be chosen to ensure that the optical quality of the laser beam is not degraded before it gets to the objective. To simplify design choices, we first choose an objective and then focus on the optical invariant of each component. By ensuring each component's optical invariant matches (or exceeds) that of the objective,

even a basic objective can yield a large FOV and a good laser spot size, resulting in a large space-bandwidth product [3]. Furthermore, sacrificing some resolution, such as by limiting the excitation numerical aperture, can lead to large FOV gains while still being able to resolve single cells. Next, each GCaMP6 mouse line has characteristic time constants and fluorescence contrast ratio for calcium binding. With these properties in hand, we design the TPM to have a high enough SNR and frame rate to image the transients effectively. Unfortunately, a large space bandwidth product requires scanning the laser quickly, limiting the pixel dwell time and therefore the SNR. Fortunately, the nonlinear nature of two-photon fluorescence means that the signal increases quadratically with laser power. Of course, increasing the power will, in turn, adversely affect fluorophore bleaching, photodamage, and thermal damage. We show that these damage mechanisms, however, all scale beneficially with increasing spot size and FOV, so the laser power can be increased safely and substantially. With these design considerations, calcium transients at the whole cortex level can be imaged with cellular resolution, see Figure 1.

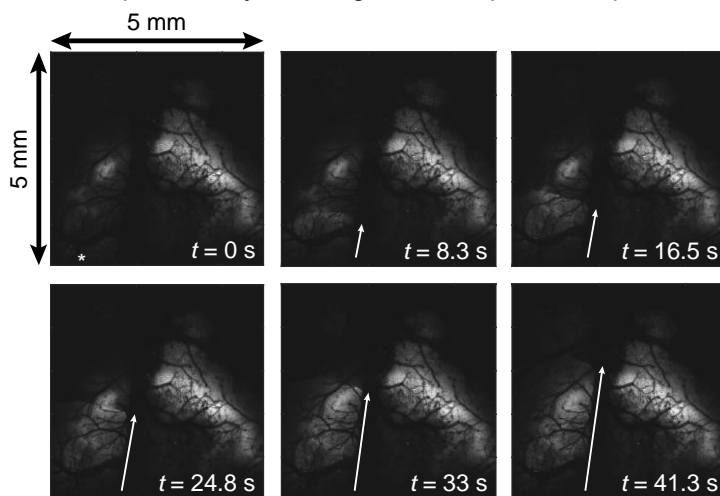


*Figure 1 – Six frames of a cortical spreading depression (CSD) measured on a mouse with a full craniotomy. The field of view is 5 mm by 5 mm, and the frame rate is 15 Hz averaged down to 3 Hz for signal clarity. In the first frame, upper left, the CSD begins at  $t = 0$  s and its location is marked with an asterisk. The CSD front propagates from posterior to anterior in the left cortex, marked by an arrow in each frame. The entire CSD lasts approximately one minute.*

1. B. White, et al., "Imaging of Functional Connectivity in the Mouse Brain," PLoS One (2011).
2. N. J. Sofroniew, et al., "A large field of view two-photon mesoscope with subcellular resolution for in vivo imaging," eLife 5 (2016).
3. J. R. Bumstead, et al., "Designing a large field-of-view two-photon microscope using optical invariant analysis," Neurophoton. 5(2), 025001 (2018).

## USING A MULTIMODAL PLATFORM TO INVESTIGATE THE ROLE OF SPREADING DEPOLARIZATIONS AND HEMODYNAMICS IN NEUROLOGICAL RECOVERY

Christian Crouzet, Beckman Laser Institute and Medical Clinic, University of California, Irvine,  
ccrouzet@uci.edu

Robert H. Wilson, Beckman Laser Institute and Medical Clinic, University of California, Irvine

Donald Lee, Department of Medicine, University of California, Irvine

Afsheen Bazrafkan, Department of Neurology, University of California, Irvine

Ayushi Patel, Department of Biomedical Engineering, University of California, Irvine

Bruce J. Tromberg, Beckman Laser Institute and Medical Clinic, University of California, Irvine

Yama Akbari, Departments of Neurology and Medicine, University of California, Irvine

Bernard Choi, Beckman Laser Institute and Medical Clinic, University of California, Irvine

Words: cardiac arrest, spreading depolarization, laser speckle imaging, spatial frequency domain imaging

Acute brain injury, such as traumatic brain injury, stroke, and subarachnoid hemorrhage exhibit spreading depolarizations (SDs). SDs have been associated with worsening neuronal injury and are thought to contribute towards overall worse neurological outcome. SDs during global cerebral ischemia and its implications on neurological recovery following reperfusion are poorly understood. We investigated the role of SDs in a global cerebral ischemia model of cardiac arrest (CA) and cardiopulmonary resuscitation (CPR).

To induce SD, rats underwent asphyxial CA (ACA) for 5-, 7-, or 8-min, which was followed by CPR. Previous studies used electrocorticography (ECoG) to detect SDs. We used a multimodal platform of ECoG, laser speckle imaging (LSI), and spatial frequency domain imaging (SFDI) to continuously monitor rats during SD and recovery. We measured brain electrophysiology, cerebral blood flow (CBF), tissue scattering, and cerebral metabolic rate of oxygen (CMRO<sub>2</sub>). Neurological outcome was measured 90min post-CPR using quantitative ECoG (i.e. information quantity (IQ)) and 24h post-CPR using behavioral tests (i.e. Neurological Deficit Score; NDS). SDs were manually detected after applying a 1Hz low-pass filter on ECoG (Fig 1A, red number 2) and with tissue scattering from SFDI (Fig 1B, bottom, spatial increase in tissue scattering from right to left).

SDs typically occurred within 2-3min after onset of asphyxia, during which vasoconstriction of cerebral vessels, waves of spreading ischemia and scattering, and abrupt changes in CMRO<sub>2</sub> were visualized. Interestingly, rats with earlier SD showed better neurological recovery (NDS) (Fig 1C). In addition to earlier SD being associated with better neurological recovery, we also found that less total CBF prior to SD (Fig 1D) and a smaller change in tissue scattering (Fig 1E) during SD were associated with better neurological recovery (ECoG IQ).

Although SDs have typically been perceived to be harmful and detrimental to neurological outcome, our data provides evidence that earlier SDs may have neuroprotective potential. These data provide support for the earliest known biomarker of neurological outcome post-CA. These findings may lead to novel therapies to modulate SDs during CA and acute brain injury that improve neurological outcome.

## METHODOLOGY TO RAPIDLY MAP AND QUANTIFY WHOLE-BRAIN MICROVASCULATURE IN 3D

Katiana Khouri, University of California, Irvine  
katianam@uci.edu

Adrian Bahani, University of California, Irvine  
Christian Crouzet, University of California, Irvine

Keywords: microvasculature, whole-brain, clearing

The role of microvasculature in the development of cerebral disorders remains ambiguous despite recent implications in ~45% of dementia cases (including Alzheimer's) and ~20% of strokes.<sup>1</sup> Our goal is to develop 3D, high resolution, whole-brain maps of the cerebral microvasculature. This will address the knowledge gap surrounding vasculature changes during disease progression and ultimately support the development of innovative treatment paradigms. This effort is complementary to the BRAIN Initiative's emphasis on comprehensive neuronal mapping. To better understand the role of vasculature in the onset of cerebral pathologies, we have developed a protocol for capture, conversion and comparison of vascular structure and key characteristics in the intact mouse brain with quotidian programs. We created a novel pipeline for 3D whole-brain modeling using techniques of perfusion for vascular labeling, amendment of the iDISCO+ organ clearing protocol, light sheet microscopy (LSM), data handling and image processing. Our protocol relies on vascular labeling via retro-orbital perfusion of fluorescent Lectin-Dylight 649 (Vector Labs), which we have observed to label vasculature in a more comprehensive fashion than other dyes (i.e., lectin-FITC, Dil). It takes up to two days to achieve whole-brain clearing; whereas the iDISCO+ protocol requires the use of secondary antibodies and a timeline of weeks. In lieu of expensive software packages, such as the Filament Tracer feature in Imaris, we trace the vasculature using freeware packages that can be used for 3D reconstruction and manipulation from most personal computers (Figure 1B). Current work involves integration of our data with the Allen Brain Atlas, to merge our vascular computational data sets to an averaged frame of reference map for use by other groups. We anticipate that this approach can be used to study the relationship between microvascular structure and function with cerebral pathology and to fit mathematical models of hypoxia predictive of ischemic conditions in the brain.

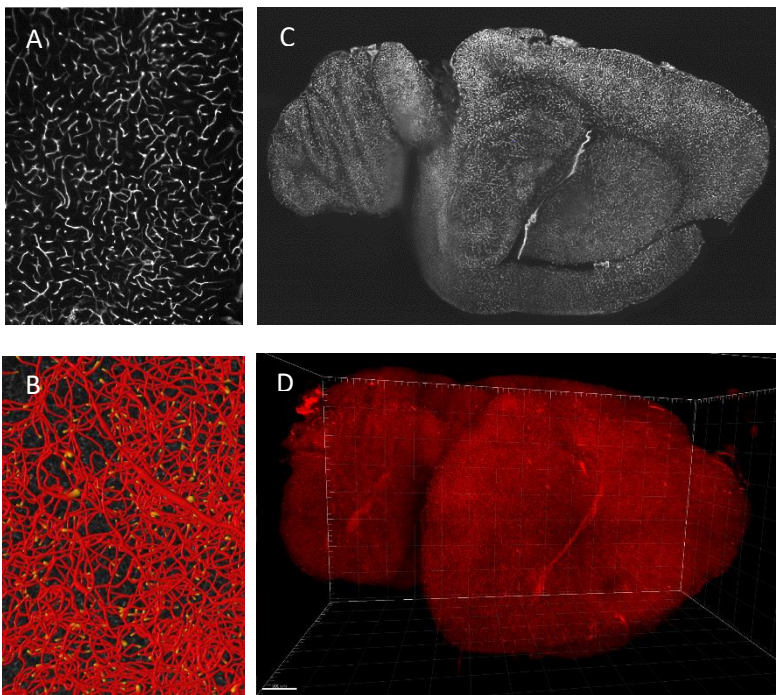


*Figure 1: Visualization and quantification of whole mouse brain vasculature using LSM: (A) Micron-resolution microvasculature structure in a single imaged plane (B) Computational tracings of one LSM 3D tile, translation to data for quantification (C) One plane of stitched tiles (D) 3D rendering of stitched whole brain vasculature*

[1] Y. Shi and J. M. Wardlaw, "Update on cerebral small vessel disease: a dynamic whole-brain disease," *Stroke Vasc. Neurol.*, vol. 1, no. 3, pp. 83–92, Sep. 2016.

## MICROVASCULAR CEREBRAL HEMODYNAMICS IN PEDIATRIC SICKLE CELL DISEASE WITH DIFFUSE CORRELATION SPECTROSCOPY

Erin M. Buckley of Emory University/Georgia Institute of Technology  
Erin.buckley@emory.edu  
Seung Yup Lee, Emory University  
Eashani Sathialingam, Emory University/Georgia Institute of Technology  
Kyle Cowdrick, Emory University/Georgia Institute of Technology  
Kendall Williams, Emory University/Georgia Institute of Technology  
Bharat Sanders, Emory University  
Courtney E. McCracken, Emory University  
Wilbur Lam, Emory University/Georgia Institute of Technology  
Clinton H. Joiner, Emory University

**Key Words:** Diffuse correlation spectroscopy, near infrared spectroscopy, cerebral blood flow, sickle cell disease

Sickle cell disease is a genetic blood disorder that has profound effects on the brain. Chronic anemia combined with both macro- and micro-vascular perfusion abnormalities that arise from stenosis or occlusion of blood vessels, increased blood viscosity, adherence of red blood cells to the vascular endothelium, and impaired autoregulatory mechanisms in sickle cell disease patients all culminate in susceptibility to cerebral infarction. Indeed, the risk of stroke is 250 times higher in children with sickle cell disease than in the general population. Unfortunately, while transcranial Doppler ultrasound (TCD) has been widely clinically adopted to longitudinally monitor macrovascular perfusion in these patients, routine clinical screening of microvascular perfusion abnormalities is challenging with current modalities (e.g., positron emission tomography, magnetic resonance imaging) given their high-cost, requirement for sedation in children < 6y, and need for trained personnel. In this pilot study, we first assess the feasibility of a low-cost, noninvasive optical technique known as Diffuse Correlation Spectroscopy (DCS) to quantify an index of resting-state cortical cerebral blood flow in 11 children with SCD along with 11 sex- and age-matched healthy controls. As expected, blood flow index was significantly higher in sickle subjects compared to healthy controls ( $p < 0.001$ ). Within sickle subjects, blood flow index was inversely proportional to resting-state arterial hemoglobin levels ( $p = 0.012$ ), consistent with expected anemia-induced compensatory vasodilation that aims to maintain adequate oxygen delivery to the tissue. Further, in a subset of patients measured with transcranial Doppler ultrasound, DCS-measured blood flow was correlated with TCD-measured blood flow velocity in middle cerebral artery ( $R_s = 0.68$ ), although the trend was not statistically significant ( $p=0.11$ ). These results are consistent with those of several previous studies using traditional neuroimaging techniques to quantify cerebral blood flow, suggesting that DCS may be a promising low-cost tool for assessment of tissue-level cerebral blood flow in pediatric sickle cell disease. Finally, given that sickle cell disease is often associated with severe anemia, we next assessed the potentially confounding effects of hematocrit on the DCS-measured blood flow index using a microfluidic tissue-simulating phantom. For a fixed flow rate in the microfluidic channels, we show that blood flow index is inversely correlated with hematocrit, and we present a means to correct the measured blood flow index for hematocrit in anemic conditions.

## SPAD BASED IMAGING OF CHERENKOV LIGHT IN RADIATION THERAPY

A Pétusseau, Dartmouth College, USA  
Arthur.f.petusseau.th@dartmouth.edu  
P Bruza, Dartmouth College, USA  
S Tisa, Micro Photon Devices srl, Italy  
S Gioux, University of Strasbourg, France  
B W Pogue, Dartmouth College, USA

Key words: Cherenkov imaging, SPAD camera, radiation therapy, dose

During radiotherapy, X-ray beams induce Cherenkov light emission in tissue as part of the dose delivery. This light can be used for dosimetry, in order to track and image the dose as it happens. The Cherenkov light levels are in the range of  $10^{-6}$  to  $10^{-9}$  W/cm<sup>2</sup>, which makes it challenging to detect in a clinical environment. However, because the radiation is pulsed in 4 microsecond bursts, time-gated acquisition of the signal allows for robust detection, even in the presence of ambient room lighting. Thus, imaging sensors for this application must be highly sensitive and must be able to time gate faster than a microsecond. In this study, the use of a solid-state detector composed of 64x32 single photon avalanche diodes (SPAD) was examined. The advantages of this technology were intra-chip amplification, superior X-ray noise rejection, and fast temporal gating of the acquisition. The results show that the SPAD camera was sensitive enough to detect Cherenkov radiation despite the 3% fill factor. 2D oversampling (x25) was also used to increase final image resolution to 320x160. In this work we demonstrate the SPAD camera performance in imaging Cherenkov emission from a tissue optical phantom and one patient undergoing radiotherapy. The SPAD camera sensors could be a viable alternative for Cherenkov imaging, as compared to current imaging methods that are mostly focused around image intensifier-based cameras and so have a range of non-linearities and instabilities which could be solved by an all solid-state camera sensor.

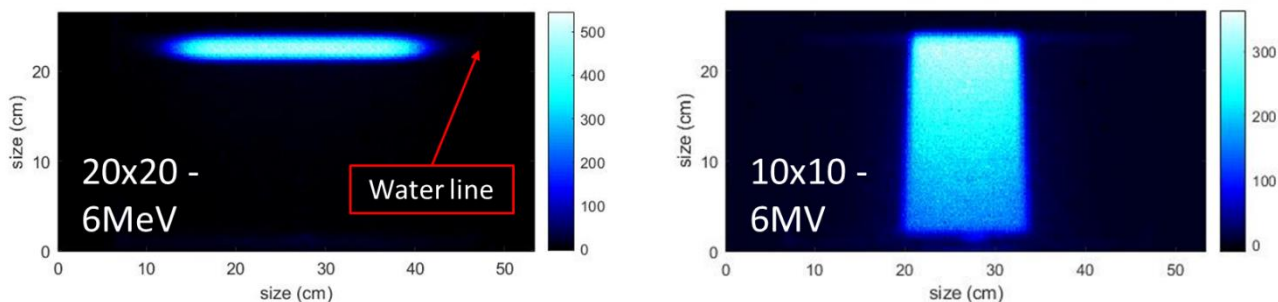


Figure 8: Water tank phantom images with different beam parameters. Left: 20x20cm electron beam, Right: 10x10cm X-ray beam.

# CHERENKOV-EXCITED LUMINESCENCE IMAGING OF MICRODOSE INJECTIONS FOR NOVEL TUMOR RESPONSE ASSAY

Jennifer Soter, Thayer School of Engineering, Dartmouth College, USA  
Jennifer.a.soter.th@dartmouth.edu

Ethan LaRochelle, Thayer School of Engineering, Dartmouth College, USA  
Brian Pogue, Ph.D., Thayer School of Engineering, Dartmouth College, USA

Key Words: Cherenkov-excited luminescence, microdose injections, imaging radiotherapy

We propose a radically new assay of tumor response to chemotherapeutic agents using microdose injections of luminescent marker inks, where the response spread of the microdose injections are readout using radiotherapy sheet illumination. In this work we characterize, in tissue-simulating phantoms, a variety of luminescent marker inks that can be detected using Cherenkov-excited luminescence imaging. Luminescent marker inks studied include commercially available UV-activated tattoo inks. Initial feasibility studies to assess the use of this novel tumor response assay demonstrate key parameters including spatial resolution, variations in inclusion size, injection spread and depth detection in tissue-simulating phantoms to show promise for further application of this technology in animals.

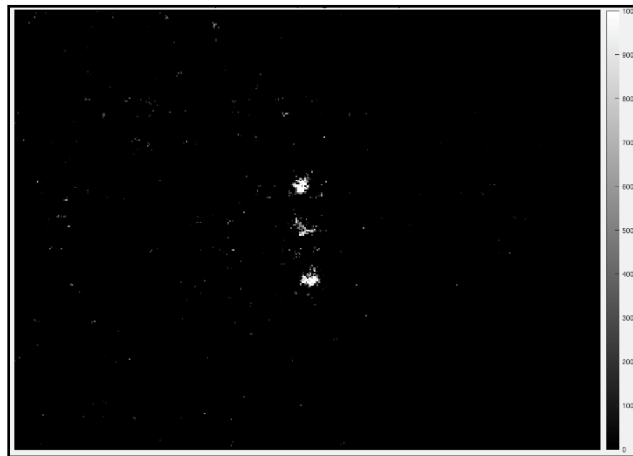


*Figure 9 – Microdose injections of luminescent marker inks in tissue-simulating phantom, imaged using Cherenkov-excited luminescence technique*

# USING DYNAMIC VASCULAR OPTICAL SPECTROSCOPY TO MONITOR PATIENTS WITH PERIPHERAL ARTERIAL DISEASE – THREE EXEMPLARY CASES

Alessandro Marone, Department of Biomedical Engineering, Columbia University, USA  
am4072@columbia.edu

Jennifer W. Hoi, Department of Biomedical Engineering, Columbia University, USA  
Christopher J. Fong, Department of Biomedical Engineering, Columbia University, USA

Youngwan Kim, Department of Electrical Engineering, Columbia University, USA

Hyun K. Kim, Department of Radiology, Columbia University, USA

Danielle R. Bajakian, Division of Vascular Surgery and Endovascular Intervention, Columbia University Irving Medical Center, USA

A.H. Hielscher, Depts. Biomed. & Electrical Engineering and Radiology, Columbia University, USA

Key Words: PAD, Optical Spectroscopy, blood flow.

In this study, Dynamic Vascular Optical Spectroscopy (DVOS) was used to monitor the blood flow in patients affected by peripheral arterial disease (PAD) who underwent lower extremity revascularization procedures. Four different angiosomes on the foot were considered, collecting point-based measurements of the vascular dynamics during a venous cuff occlusion (@ 60 mmHg) in the lower extremity with the system shown in Fig. 1.

Over 70 patients were monitored from before the intervention to up to one year later. Among them, we selected 3 exemplary cases that can highlight different hemodynamics flows in the foot of these patients. The general idea behind our research is that if a patient has a healthy vasculature, when we interrupt the venous return using a thigh cuff occlusion the saturation of the blood in the foot will be swifter than in the case of a patient in which its arterial tree is occluded and less blood can pool in the lower extremities.

In the first example, the patient had a very poor blood flow in the foot which caused an ulcer to develop. After the intervention (angioplasty of MPA) this ulcer completely healed in less than 3 months. It is possible to see from Fig. 2-A that the difference between the state pre-intervention and two hours later was mostly maintained after 1 and 3 months. In the second case, the patient had to have a 2<sup>nd</sup> intervention (bypass surgery) 5 weeks after the 1<sup>st</sup> intervention since the first by-pass failed. It is in fact possible to see from Fig. 2-B that the situation 1 month after the first intervention deteriorated and the optical data suggested a situation even worse than before the first intervention.

Finally, in the third case (Fig. 2-C), the patient showed a good recovery and few months of wellbeing after an angioplasty of the LMP. But after about 6 months, the situation reverted to the pre-intervention state and in fact the patient started claudicating and feeling pain in the foot comparable to the situation before the intervention. This is reflected by the optical signal reverting back to the pre-intervention state.



system used to obtain DVOS measurements.

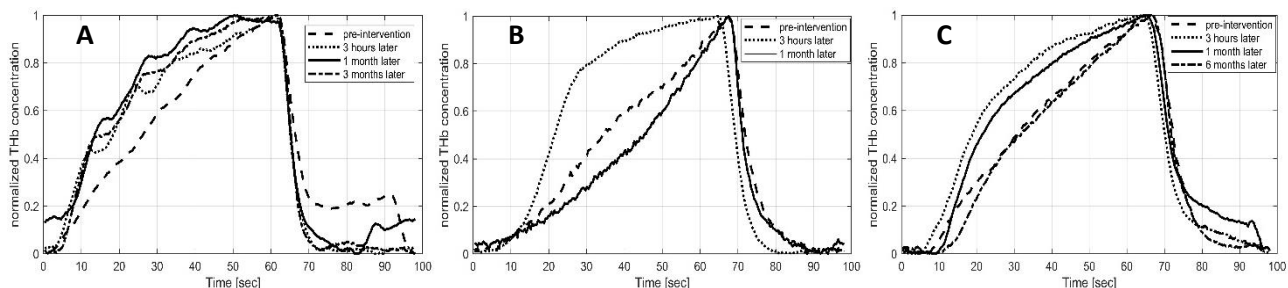


Figure 2 – Three exemplary cases (A,B,C) of PAD patient who had an endovascular intervention. In the graphs, the normalized total hemoglobin concentration reconstructed from the optical signals collected with our DVOS system are shown.

As shown in these three cases, there is a direct correlation between the optical signals collected with DVOS and the hemodynamic responses to a venous cuff occlusion in the foot of the patients affected by PAD: lower blood flow causes longer times for the optical signal to saturate and reflects a state of poor vascular conditions.

## **IMAGING OF STIFFNESS HETEROGENEITY IN PANCREATIC CANCER TO ASSESS ELASTOGRAPHY AS A SURROGATE FOR DRUG DISTRIBUTION IN ORTHOTOPIC XENOGRAFT MODELS**

Phuong Vincent, Dartmouth College, USA  
phuong.d.vincent.th@dartmouth.edu

Limited systemic delivery in solid tumors has greatly reduced the efficacy of most therapeutic options in pancreatic ductal adenocarcinoma (PDAC). The excess of desmoplasia in PDAC tumor microenvironment elevates total tissue pressure, which is often measured via solid stress and interstitial fluid pressure. While these two factors are well-studied to characterize their influence on limited diffusion and convection transport in solid tumors, the nature of point-probe based measurements makes it difficult to assess the heterogeneous profile of tissue pressure. Therefore, this study aimed to explore tissue stiffness as an alternative biological parameter that has the potential of being a non-invasive measurement as well as having the resolution to detect tissue heterogeneity in PDAC. An ex vivo stiffness mapping system was developed which included a motorized xyz table and a fiber optic pressure sensor operated by a micro-opto-mechanical system. The motorized table tracked the spatial coordinates of the sensor as it moved along the tissue surface to independently map out stiffness at 300 micron resolution. At each location, the sensor measured pressure based on a 3-step loading test to determine stiffness. This stiffness mapping system was calibrated with ultrasound elastography to produce absolute Young's modulus values. The study has showed that stiffness heterogeneity in two orthotopic xenograft models, AsPC-1 and BxPC-3, was strongly correlated with collagen content in the tumors. The inverse correlation between stiffness and vascular patency highlighted the feasibility of using stiffness to predict drug penetration in PDAC tumors. Texture analysis to evaluate collagen thickness and structure were performed to further explore the cause of heterogeneity in pancreatic tumor microenvironment across different tumor lines.

## TOTAL HEMOGLOBIN REDUCTION IN THE TUMOR VOLUME CORRELATES WITH RESPONSE TO BREAST CANCER NEOADJUVANT CHEMOTHERAPY WITHIN TWO WEEKS OF TREATMENT

Mirella Altoe, Dept. Biomedical Engineering, Columbia University, USA  
ma3477@columbia.edu

Alessandro Marone, Dept. Biomedical Engineering, Columbia University, USA  
Hyun K. Kim, Dept. Radiology, Columbia University, USA

Mariella Tejada, Herbert Irving Comprehensive Cancer Center, Columbia University, USA  
Hanina Hibshoosh, Dept. Pathology, Columbia University, USA

Katherine Crew, Dept. Medicine - Hematology/Oncology, Columbia University Medical Center, USA

Kevin Kalinsky, Dept. Medicine - Hematology/Oncology, Columbia University Medical Center, USA

Dawn L. Hershman, Dept. Medicine - Hematology/Oncology, Columbia University Medical Center, USA

Andreas H. Hielscher, Dept. Biomedical & Electrical Engineering and Radiology, Columbia University, USA

Key Words: tumor response, neoadjuvant chemotherapy, breast cancer, diffuse optical tomography.

Optical imaging techniques have emerged as a possible alternative to predict pathological complete response (pCR) in breast cancer patients undergoing neoadjuvant chemotherapy (NAC). Our team developed a so-called diffuse optical tomographic breast imaging system (DOTBIS) which does not require the use of contrast agents or compression, and enables imaging of the whole breast volume using low intensity near infrared light capable to measure tissue concentration of oxy-hemoglobin (ctO<sub>2</sub>Hb), deoxy-hemoglobin (ctHHb) and water percentage. In this retrospective study, ctTHb changes in the tumor region of 16 breast cancer patients were analyzed across NAC. Both breasts of all patients have been scanned simultaneously with our DOTBIS system, Figure 1, which employs four wavelengths and gathers data from a total of 64 sources and 128 detectors per breast. A PDE-constrained multispectral image reconstruction code creates 3D image maps of total hemoglobin (ctHbT = ctO<sub>2</sub>Hb+ ctHHb). Tumor volume is selected by entering radiologic information such as tumor side, clock position and distance from the nipple (FN). An automated code was designed to select the



Figure 10 – Photograph of the custom-built diffuse optical tomographic breast imaging system (DOTBIS).

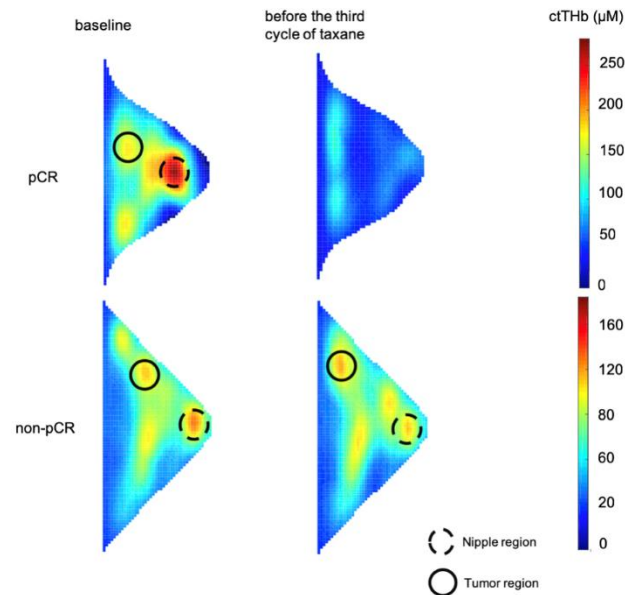


Figure 2 – Comparison between a pCR and non-pCR patient at baseline and before the third cycle of taxane. We see a significant reduction in ctTHb right after the second taxane drug cycle in the tumor region (filled circle line) for the pCR patient. Nipple region is identified by the dashed circle line.

highest value from the distance FN and the quadrant referent to the clock position. Subsequently, a region-based image segmentation method is implemented to examine neighboring pixels of the highest value point considering a mask of 90%. After tumor volume segmentation, we calculate the mean ctHbT extracted from the region of interest. An independent-samples t-test was run to determine if there were differences in ctTHb reduction in the tumor region before the third cycle of taxane between responders (n=4) and non-responders (n=12). ctTHb reduction was greater to pCR ( $45.71 \pm 25.16 \mu\text{M}$ ) than non-pCR tumors ( $-9.67 \pm 25.65 \mu\text{M}$ ), a statistically significant difference of  $55.38 \mu\text{M}$  (95% CI, 23.74 to 87),  $t(14) = 3.755$ ,  $p = .002$ , in Figure 2 we can see an example. From the ROC plot results, we can observe that ctTHb reduction in the tumor region after 2 cycles of Taxane is a good indicator to anticipate pCR status. With an area under the curve of 0.958, the best cut-off that maximizes sensitivity and specificity is  $16.86 \mu\text{M}$ . At this reduction level, the sensitivity is 100% and specificity is 91.7%. In conclusion, our findings indicate that DOTBIS-measured total hemoglobin in the tumor region may be a strong and independent predictor of treatment response to NAC.

## WEARABLE TOE BAND SYSTEM FOR MONITORING OF PERIPHERAL ARTERY DISEASE

Youngwan Kim, Dept. of Electrical Engineering, Columbia University, New York, NY, USA  
yk2561@columbia.edu

Alessandro Marone, Dept. of Biomedical Engineering, Columbia University, New York, NY, USA  
Hyun K. Kim, Dept. of Radiology, Columbia University Irving Medical Center, New York, NY, USA  
Danielle Bajakian, Columbia University Irving Medical Center, New York, NY, USA

Ioannis Kymissis, Dept. of Electrical Engineering, Columbia University, New York, NY, USA  
Andreas H. Hielscher, Depts. of Biomedical & Electrical Engineering and Radiology, Columbia University

**Key Words:** wearable optical imaging band system, dynamic diffuse optical spectroscopy, peripheral artery disease

Approximately 8 to 12 million people in the United States suffer from peripheral artery disease (PAD). PAD causes narrowed arteries and reduces blood flow to the lower extremities. People with PAD begin to experience discomfort and pain while walking. Untreated PAD can lead to ulcers, gangrene, and amputation. Before experiencing those severe conditions, detection of narrowing blood vessel enables early diagnosis and treatment. Therefore, accurate and timely diagnosis is necessary.

We have developed a low-cost wearable imaging band system that employs dynamic diffuse optical spectroscopy (dDOS) technique. The system includes 4 different measurement modules that each has a pair of three light-sources and a single Si-photodetector. The three light-source consists of light emitting diodes (LEDs) operating at wavelengths of 530, 655, 940 nm. When an individual light source is on, four detectors at different spots around a toe read the intensities of diffusely reflected and transmitted light. The intensity of light is converted to a voltage and amplified by transimpedance amplifier (TIA). The digitized data is transferred to a computer by microcontroller and embedded system.

We have used the system in a clinical pilot study with 10 PAD patients that undergo an endovascular intervention. The wearable imaging band accesses PAD patients 1 hour before and 1 hour after angioplasty.

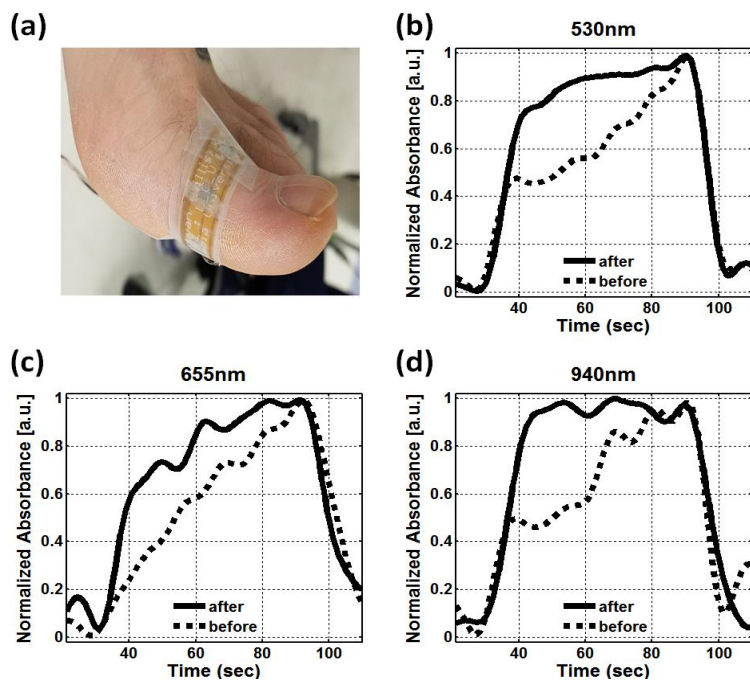


Figure 11. Wearable imaging band wrapped around a toe (a) and change of absorbance of three wavelengths (530 nm (b), 655 nm (c), 940 nm (d)), measured before and after angioplasty at a thigh cuff occlusion of 100 mmHg from Peripheral Artery Disease (PAD) patient.

High pressure cuff occlusions at 60 mmHg and 100 mmHg are applied for 60 seconds each, and the changes in light transmission are recorded. During the thigh cuff occlusion, the blood volume in the extremities is changed leading to a change in the measured signal. An example for a patient whose medial plantar artery (MPA) was treated is shown in Figure 1. The wearable imaging band wrapped around the patient's toe is shown in Figure 1 (a). Figure 1 (b), (c), and (d) show absorbance changes of wavelengths at 530, 655, and 940 nm respectively during a 100 mmHg occlusion. Absorbance before angioplasty (dotted line) reaches the max value more slowly than after receiving an angioplasty (solid line). We hypothesize that in untreated patients the narrowed MPA can only respond slowly to the cuff. The treated MPA has a larger lumen and hence the blood pooling in a toe increases much faster during thigh occlusion. Similar results were found in all 10 patients.

We have shown that the wearable imaging band system can detect differences between hemodynamics before and after angioplasty. The wearable form factor

should allow for integration in home-based monitoring systems, where it could potentially be used to assess the status of the vasculature. Therefore, early diagnosis and monitoring of PAD in daily life may be possible.

## WORKFLOW FOR REAL-TIME IN-VIVO CHERENKOV-EXCITED LUMINESCENCE IMAGING DURING RADIOTHERAPY

Ethan LaRochelle, Thayer School of Engineering at Dartmouth College  
ethan.phillip.m.larochelle.th@dartmouth.edu

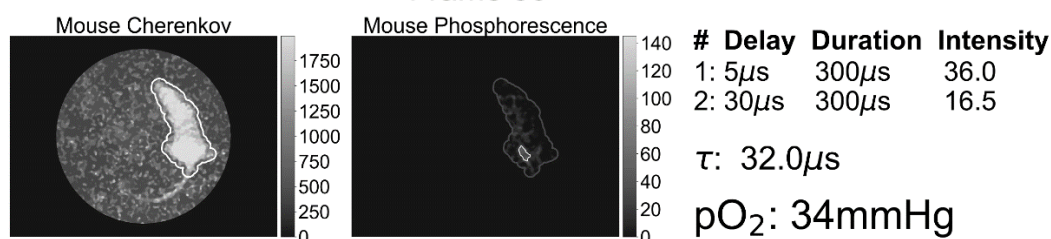
Jennifer Shell, Thayer School of Engineering at Dartmouth College  
Jason Gunn, Thayer School of Engineering at Dartmouth College  
Michael Jermyn, DoseOptics

Sergei Vinogradov, Department of Biochemistry and Biophysics at University of Pennsylvania  
Brian Pogue, Thayer School of Engineering at Dartmouth College

**Key Words:** Cherenkov Luminescence imaging, Radiotherapy, Phosphorescence lifetime imaging, Oxygen sensing, tumor hypoxia

Radiotherapy is a common method for treating tumors, however, radiosensitivity can vary between tumor types or within the tumor microenvironment. The ability to deliver oxygen is crucial for the generation of reactive oxygen species resulting in increased localized cytotoxic effects. Alternatively, hypoxic tumors are thought to indicate a poor prognosis and may benefit from more aggressive treatments, yet identifying tumor hypoxia early in the course of a multi-week fractionated dose regimen is currently impractical. Using a time-gated imaging system and oxygen-sensitive phosphorescent compound (PtG4) we are able to estimate *in vivo* pO<sub>2</sub> distribution at a rate of 2.6 estimates per second, which corresponds to 50+ values during a common 2Gy dose fraction. While our previous work has reported using Cherenkov-excited luminescence to estimate *in vivo* pO<sub>2</sub> during external beam radiotherapy, the dose required was often greater than a standard fraction and camera acquisition parameters required modification during treatments, resulting in interrupted workflows. The current method utilizes custom control software which cycles through camera timing parameters during acquisition. Python code using the web-based user interface JupyterLab allows for interactive analysis of the resulting image stack without the need to pay expensive licensing fees for scientific computing packages. Using open source libraries, the analysis code is able to split the image stack into respective Cherenkov excitation and phosphorescence images, which can then be further automatically segmented to find regions of interest including the subject and phosphorescent region. The intensity of the regions in the phosphorescence images are used to estimate the compound lifetime, which can then be used in the Stern-Volmer relationship to estimate pO<sub>2</sub>. This entire process does not compromise clinical workflow and is able to provide a pO<sub>2</sub> estimate within minutes after delivering the fractionated dose, providing clinicians early feedback about trends in tumor hypoxia. The current method has been validated with both direct injection of 50μM PtG4 in Matrigel in a mouse flank, and 24hrs post IV injection of mouse with MDA-MB-231 tumor implanted in the flank. The mouse with the direct injection was imaged under anesthesia and while awake and mobile to test the ability of the automated segmentation algorithm (Figure below). While the signal from the IV injection was less intense, simultaneous imaging using the previously reported method and current method resulted in similar lifetime estimates. While oxygen-sensitive PtG4 exhibits a lifetime between 16μs under atmospheric oxygen and 47μs when deprived of oxygen, other compounds have also been investigated. Europium chelate nanoparticle (~600μs), Iridium-based small molecules (~5μs), Si nanoparticles (~60μs), and UV-sensitive tattoo inks (~15μs) have all been imaged using Cherenkov-excitation. Camera time-gating can be utilized to discriminate these compound when mixed in the same field, allowing for additional tools in the realm of contrast enhancement during radiotherapy imaging. Ongoing studies with PtG4 and other compounds are being conducted to further improve system sensitivity and refine imaging workflows so they are more clinically translatable.

Frame 50



Automatic segmentation to determine pO<sub>2</sub> of PtG4 implanted in Matrigel in the flank of an unanesthetized freely-moving nude mouse. (Left) Cherenkov image of the mouse where the white outline was determined programmatically. (Right) Phosphorescence image collected 5μs after the X-ray pulse, where the white outline shows the region more than one standard deviation above the mean mouse phosphorescence. (Right) Two phosphorescence intensities can be used to find a lifetime of 32μs which corresponds to a pO<sub>2</sub> of 34 mmHg.

**TOWARDS LABEL-FREE IMAGING OF BREAST CANCER-INDUCED PRE-METASTATIC NICHE  
USING SPONTANEOUS RAMAN SPECTROSCOPY**

Santosh Kumar Paidi, Johns Hopkins University, USA  
santoshpaidi@jhu.edu